PERGAMON

International Journal of Heat and Mass Transfer 42 (1999) 2571–2581

International Journal of HEAT and MASS TRANSFER

Chaotic mixing and mass transfer enhancement by pulsatile laminar flow in an axisymmetric wavy channel

B.S. Lee[a], I.S. Kang[a,*], H.C. Lim[b]

[a] *Department of Chemical Engineering, Pohang University of Science and Technology, San 31, Hyoja Dong, Pohang, 790-784, Republic of Korea*

[b] *Department of Chemical and Biochemical Engineering and Material Science, University of California, Irvine, CA 92697, U.S.A.*

Received 20 April 1998; in final form 2 October 1998

Abstract

Mass transfer enhancement by a pulsatile laminar flow in an axisymmetric wavy channel has been investigated numerically for the range of $50 \leqslant Re \leqslant 250$ and $0.1 \leqslant St \leqslant 10$. The optimal Strouhal number has been determined as a function of the Reynolds number and the wavelength of the channel. It is found that the optimal Strouhal number increases weakly as the Reynolds number decreases. It is also found that the optimal Strouhal number is almost inversely proportional to the channel wavelength. For better understanding of the enhancement mechanism, the Lagrangian flow analysis has also been performed. For an efficient computation, the Eulerian velocity field is represented by the Fourier series. Particle trajectories show chaotic behaviors when the Strouhal number is close to the optimal value. It is observed that there is a very strong correlation between the mass transfer enhancement factor and the average Lagrangian Lyapunov exponent.

Nomenclature

$\tilde{C}$ concentration [kg mole m^{-3}]
D mass diffusivity [$m^2\ s^{-1}$]
E mass transfer enhancement factor, dimensionless
$\tilde{R}$ maximum radius of axisymmetric wavy channel [m]
Re Reynolds number
Sc Schmidt number
Sh Sherwood number defined by equation (7)
$\langle Sh \rangle_t$ spatio-temporal mean Sherwood number defined by equation (8)
St Strouhal number
u_r radial velocity, dimensionless
u_x axial velocity, dimensionless
$u^o_{i,j}$ original velocity at grid point (i,j), dimensionless
$u^r_{i,j}$ reconstructed velocity at grid point (i,j), dimensionless
u_ξ ξ-directional velocity in the orthogonal curvilinear coordinate system
u_η η-directional velocity in the orthogonal curvilinear coordinate system.

Greek symbols
α^2 pulsatile Reynolds number in equation (6)
γ geometric amplitude
ε dimensionless flow amplitude in equation (6)
λ_L finite-time Lagrangian Lyapunov exponent
$\bar{\lambda}_L$ average Lagrangian Lyapunov exponent
$\tilde{\Omega}_h$ radian frequency of pulsation [s^{-1}]
Ω_w dimensionless geometric wave number divided by π
$\tilde{\Omega}_w$ dimensional geometric wave number divided by π [m^{-1}].

1. Introduction

Heat and mass transfer enhancement by pulsatile flows is of great importance and has been studied numerically and experimentally by many investigators. From previous studies, it is known that the pulsation of fluid flow alone in a straight channel has little effect on heat and mass transfer. Thus the heat and mass transfer enhancement in a channel with periodically modified geometry has attracted attention.

As a way of geometry modification, a channel with periodic square groove has been considered. Patera and

* Corresponding author.

0017–9310/99/$ - see front matter
PII: S0017–9310(98)00349–4

Mikic [1] performed experiments to observe the resonant heat transfer enhancement by excitation of shear-layer instabilities. Ghaddar et al. [2, 3] studied the same problem by numerical investigation and found strong resonant nature of response to small fluid oscillations near the natural frequency. However, their non-smooth geometry results in higher pressure drop. On the other hand, Nishimura et al. [4] performed experiments for the flow and mass transfer characteristics in sinusoidal wavy 2-D channel for a purely oscillating flow. Although they observed mass transfer enhancement, they could not find any significant effect of the oscillating frequency because the range of the Strouhal number in their experiments was too low. Later, Nishimura and Kojima [5] reconsidered the pulsatile flow in a wavy channel to see the effects of net flow, amplitude and frequency of oscillation.

Fluid mixing has been considered as one of the key factors in heat and mass transfer enhancement. Thus, there have been quite extensive works for understanding of mixing mechanism itself in wavy channels [6–14]. Sobey and his co-workers [6–8] studied the oscillating flow in a furrowed channel with special attention to the steady streaming effect and vortex ejection. Recently chaos theory has been applied to improve the understanding and exploitation of fluid mixing [15]. In that direction, Guzman and Amon [13] used modern dynamical system techniques for the analysis of flow in the wavy channel. They used the concepts such as autocorrelation function, pseudo space representations, Poincaré sections, etc. Amon et al. [14] analyzed the characteristics of converging–diverging channel flows with view points of the Lagrangian and Eulerian chaos and their relationship to the mixing enhancement.

In the present work, we study numerically the problem of chaotic mixing and mass transfer enhancement by pulsatile laminar flow in an axisymmetric wavy channel. As we have seen above, there have been considerable works on the mass transfer enhancement by the pulsatile flow in wavy channel. However, there remain several points to be studied further. Nishimura and Kojima [5] observed experimentally that the mass transfer is enhanced as the oscillation frequency is increased, but they could not find the optimal frequency due to the parameter range adopted in their study. This point provides the first movitation of our work. In the first part of our work, we find the optimal oscillation frequency, which is represented by the optimal Strouhal number, as a function of the Reynolds number and the wavelength of the wavy channel. The next objective is to find a relationship between the mass transfer enhancement and the Lagrangian flow characteristics. For an efficient computation, the Eulerian velocity field is represented by the Fourier series and the average finite-time Lagrangian Lyapunov exponent is computed by using the method of Amon et al. [14]. As will be shown later, it is observed that there is a strong correlation between the mass transfer enhancement factor and the average Lagrangian Lyapunov exponent.

2. Problem statement

We are interested in the pulsatile laminar flow and mass transfer in an axisymmetric wavy channel. The governing equations are the continuity, the momentum, and the mass transfer equations. We assume laminar flow of incompressible Newtonian fluid with constant properties such as density, viscosity, and diffusivity. The schematic of the axisymmetric wavy channel is shown in Fig. 1, where γ is the dimensionless geometric amplitude define by $\gamma = \tilde{H}/\tilde{R}$ and $\tilde{\Omega}_w$ is the dimensional geometric wave number divided by π. They are defined in the equation

$$\tilde{r} = \tilde{R}[(1-\gamma)+\gamma\cos(\tilde{\Omega}_w \pi \tilde{x})] \tag{1}$$

where $\tilde{R}$ is the maximum radius of the channel.

In order to nondimensionalize the governing equations, the following characteristic scales are introduced:

$$u_c = \bar{u}_{max}, \quad l_c = \tilde{R}, \quad t_c = \frac{1}{\tilde{\Omega}_h}, \quad p_c = \rho u_c^2,$$

$$C_c = \tilde{C}_i - \tilde{C}_w$$

where $\bar{u}_{max}$ is the time-averaged velocity at the center of the entrance plane of the channel, $\tilde{\Omega}_h$ is the radian frequency of the imposed pulsatile flow, $\tilde{C}_i$ is the inlet concentration, and $\tilde{C}_w$ is the wall concentration. All variables are normalized directly by the characteristic values except for the dimensionless concentration which is defined as $c = (\tilde{C} - \tilde{C}_w)/(\tilde{C}_i - \tilde{C}_w)$. For the governing equations, we have the continuity equation

$$\nabla \cdot \mathbf{u} = 0 \tag{2}$$

the momentum equation

$$St\frac{\partial \mathbf{u}}{\partial t} + \mathbf{u}\cdot\nabla\mathbf{u} = -\nabla p + \frac{1}{Re}\nabla^2\mathbf{u} \tag{3}$$

and the mass transfer equation

$$St\frac{\partial c}{\partial t} + \mathbf{u}\cdot\nabla c = \frac{1}{Re\,Sc}\nabla^2 c. \tag{4}$$

In (3), we have two important flow parameters which are

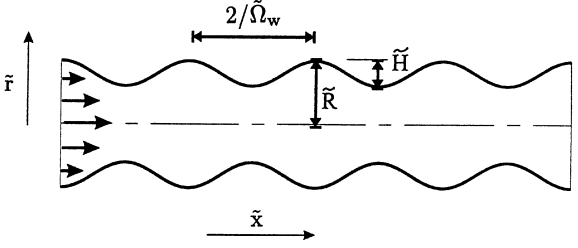

Fig. 1. An axisymmetric wavy channel where $\tilde{\Omega}_w$ is the geometric wave number divided by π and $\tilde{H}/\tilde{R}$ is the dimensionless amplitude denoted by γ in equation (1).

the Reynolds number, Re, and the Strouhal number, St. The Reynolds and the Strouhal numbers are defined as

$$Re = \frac{u_c l_c}{\nu}, \quad St = \frac{\tilde{\Omega}_h l_c}{u_c} \tag{5}$$

and the Schmidt number in (4) is defined as $Sc = \nu/D$.

For the analyses of flow field and heat and mass transfer in a wavy channel, most of the previous workers [2, 3, 6, 9] considered the section of one period and applied the fully developed condition. In the present work, differently from previous workers, we consider the section of wavy channel with several periods as our problem domain. As the boundary conditions for the flow fields, we use the following conditions. On the solid surface (hereinafter denoted by $\partial\Omega_1$), no slip condition holds. At the inlet ($\partial\Omega_2$), the pulsatile velocity profile is imposed. The unsteady pulsatile velocity profile imposed at the channel inlet will be discussed in more detail shortly. The symmetry condition holds for the center line ($\partial\Omega_3$). For the outlet condition ($\partial\Omega_4$), we assume that flow field is periodically fully-developed in the sense that the velocity profile at the outlet is identical to that at one wavelength preceding section. For the boundary conditions of the mass transfer equation, we have the constant wall concentration $c = 0$ on $\partial\Omega_1$ and the inlet condition $c = 1$ on $\partial\Omega_2$. At the symmetry axis ($\partial\Omega_3$), as in the flow field computation, the symmetry condition is used. At the exit ($\partial\Omega_4$), we impose the fully-developed condition ($\partial C/\partial x = 0$).

As the dimensionless velocity profile at inlet, we use

$$u_x = \left[(1-r^2)+\varepsilon\left\{(1-r^2)\sin t - \frac{\alpha^2}{4}\left(\frac{3}{4}-r^2+\frac{r^4}{4}\right)\cos t\right\}\right]; \quad u_r = 0 \tag{6}$$

which includes two parameters α^2 and ε. The fixed value $\alpha^2 = 37.75$ is used for all our computations and two values of $\varepsilon = 0.2$ and 0.1 have been used. When $\alpha^2 = 37.75$ and $\varepsilon = 0.2$, the velocity profile has quite interesting features as shown in Fig. 2. It shows the backward flow characteristics and it is asymmetric with respect to $t = \pi$. If the oscillation amplitude is reduced to $\varepsilon = 0.1$, there is no backward flow.

A comment may be given to the velocity profile in (6). Originally it is the asymptotic solution for the pulsatile flow in a straight channel driven by the time-periodic pressure gradient $-(\partial\tilde{p}/\partial\tilde{x}) = \tilde{G}_0[1+\varepsilon\sin(\tilde{\Omega}_h\tilde{t})]$ for the case of $\alpha^2 = l_c^2\tilde{\Omega}_h/\nu \ll 1$ (see Leal [16]). In that case, α^2 is called the pulsatile Reynolds number and ε the flow amplitude. Of course, for large values of α^2, (6) does not have meaning as the asymptotic solution. However, as we have seen in Fig. 2, it does show quite interesting flow characteristics which is similar to those of pulsatile blood flow. Thus it has been adopted as the imposed inlet velocity profile by considering α^2 and ε as just parameters in the analysis of blood flow in an artery [10].

In order to measure the transport characteristics in the pulsatile flow, we define the Sherwood number as

$$Sh = \frac{1}{A}\int_A\left[-\frac{\partial c}{\partial n}\right]dA = \frac{1}{A}\int_A\left[-\frac{1}{h_\eta}\frac{\partial c}{\partial \eta}\right]dA \tag{7}$$

where A is the dimensionless mass transfer surface area and η is the coordinate of the orthogonal (ξ, η) coordinate system for numerical analysis (see next section). The spatio-temporal mean Sherwood number is now defined as

$$\langle Sh\rangle_t = \frac{1}{T}\int_0^T Sh\,dt \tag{8}$$

where T is the dimensionless period of the imposed pulsatile flow (in this work, $T = 2\pi$). The mass transfer enhancement factor E is defined as

$$E = \frac{Sh_{unsteady}}{Sh_{steady}} = \frac{Sh(St,Re,Sc,\varepsilon)}{Sh(Re,Sc,\varepsilon = 0)} \tag{9}$$

where $Sh_{unsteady}$ is equal to $\langle Sh\rangle_t$. Note that the reference state is the steady state in which there is no oscillation at all. Thus, $Sh_{unsteady}$ does not necessarily approach Sh_{steady} even in the limit $St \to 0$. The reason is that the flow field is still oscillating with very low frequency in the case of pulsatile flow, while the flow field at steady state is fixed with respect to time.

3. Numerical methods

For the solution of Eulerian flow field equations and the mass transfer equation, we have used the finite difference method with the boundary-fitted orthogonal grid generation method. For generation of the orthogonal grid systems, we have used the method developed by Oh and Kang [17]. The grid systems generated for several geometric wave numbers are shown in Fig. 3, where the grid line in the flow direction is the ξ-coordinate and the grid line orthogonal to it is the η-coordinate of the (ξ, η)-coordinate system. The geometric amplitude γ in equation (1) was chosen to be 0.2. For most of our computation 81×21 grid systems have been used. The effects of grid resolution on the accuracy of solution were tested by using 121×31 and 161×41 systems and it was found that 81×21 system has sufficient resolution for the purpose of present study.

Since the problem is axisymmetric, the stream function and vorticity formulation is used for the flow field analysis. As the time marching scheme, the ADI scheme is used for the solution of the vorticity equation with the full convergence of the solution of the stream function equation at each time step. The detailed numerical scheme for the unsteady flow field is available elsewhere [10]. The unsteady mass transfer equation is also solved by using the ADI scheme. In order to make sure that the periodicity of the solution of the mass transfer equation is fully achieved, the following convergence criterion is used.

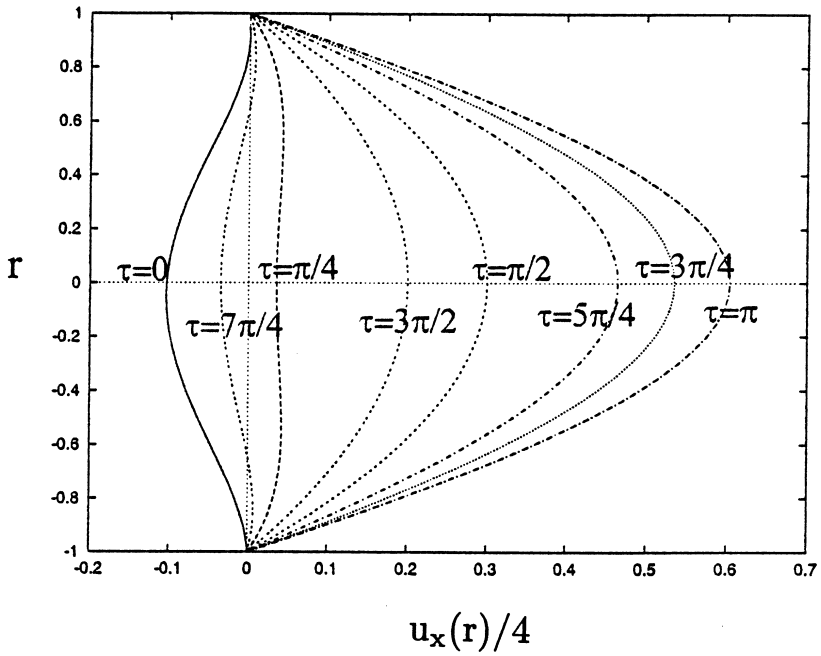

Fig. 2. Inlet velocity profile during one period ($T = 2\pi$) predicted by equation (6) with $\alpha^2 = 37.75$ and $\varepsilon = 0.2$.

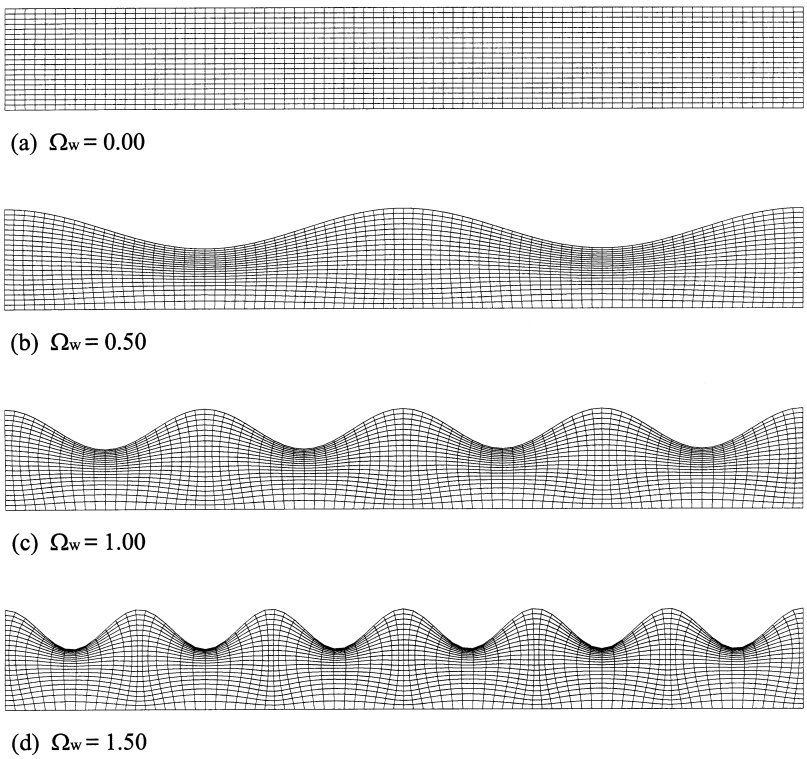

Fig. 3. Orthogonal grid systems for axisymmetric wavy channels with different geometric wave numbers Ω_w.

$$\langle Sh\rangle_t|_{(n+2)\pi} - \langle Sh\rangle_t|_{n\pi} < 10^{-3} \tag{10}$$

where $\langle Sh\rangle_t|_{n\pi}$ is the spatio-temporal mean Sherwood number for the time interval $[(n-1)\pi,\ n\pi]$ and $\langle Sh\rangle_t|_{(n+2)\pi}$ is for $[n\pi,\ (n+2)\pi]$.

As mentioned in the Introduction, one of the objectives of the present work is to perform Lagrangian flow analysis for better understanding of the mass transfer enhancement. In general the Lagrangian flow analysis is based on the particle trajectories obtained by integrating

$$\frac{d\mathbf{x}}{dt} = \mathbf{u}(\mathbf{x}, t) \tag{11}$$

where $\mathbf{u}(\mathbf{x}, t)$ is the velocity field obtained by the Eulerian flow field computation. In order to supply the Eulerian flow field data in (11) efficiently, we use the Fourier series representation of the flow field. Based on the fact that the flow field is 2π-periodic, the velocity component at each grid point (i,j) can be represented as

$$u_{i,j}(t) = \frac{A_0}{2} + \sum_{k=1}^{\infty} (A_k \cos kt + B_k \sin kt) \tag{12}$$

where u is u_ξ or u_η. The coefficients in (12) are obtained by numerical integration of the orthogonality relations, in which the time periodic numerical solution is used. The advantage of the present approach is that we can perform the integration of the orthogonal relations along with the time marching of the numerical solution of the flow field. Thus, we need to memorize only the numerical solutions at the current time step and the previous time step for integration.

The behaviors of the Fourier coefficients for u_η at a typical grid point (20, 15) are shown in Fig. 4 for the case of $\Omega_w = 1$, $Re = 250$, and $St = 1$. The convergence is excellent and they become $O(10^{-4})$ after the 20th mode, and $O(10^{-5})$ after the 30th mode. After obtaining the coefficients, we reconstruct the velocity field whenever

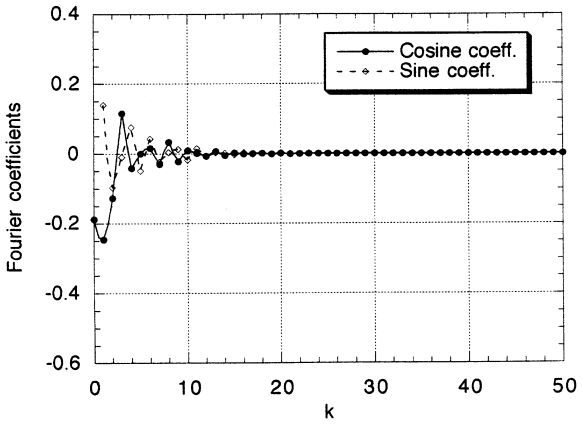

Fig. 4. Fourier coefficients for u_η at the grid point (20, 15) when $Re = 250$ and $St = 1$.

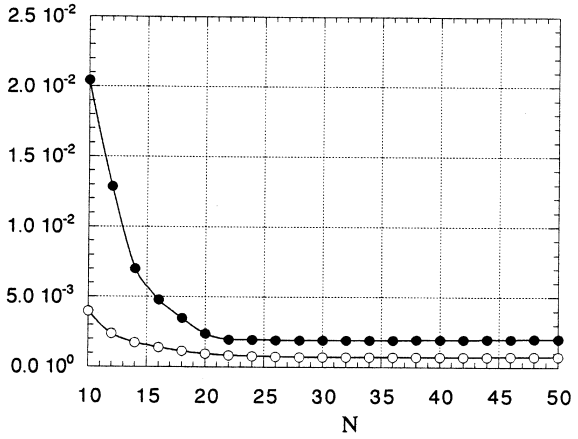

Fig. 5. The error norm as a function of mode numbers. The closed circles are for the maximum error norm $\|u^o_{i,j} - u^r_{i,j}\|_{\max}$ and the open circles for the average error norm $\|u^o_{i,j} - u^r_{i,j}\|_{\text{avg}}$.

we want. The reconstruction is done by using the finite number of terms as

$$u^r_{i,j}(t) = \frac{A_0}{2} + \sum_{k=1}^{N} (A_k \cos kt + B_k \sin kt). \tag{13}$$

In order to see the accuracy of the reconstructed velocity field, we use the error norm defined by

$$\|u^o_{i,j} - u^r_{i,j}\| = \sqrt{\frac{1}{2\pi}\int_0^{2\pi} (u^o_{i,j} - u^r_{i,j})^2\, dt} \tag{14}$$

where $u^o_{i,j}$ is an original velocity signal at grid point (i,j). The accuracy of the reconstructed velocity field is checked by the maximum value and the average value of the norm over all grid points. The result is shown in Fig. 5, which shows that the series with $N = 30$ gives a reconstruction with sufficient accuracy. Thus, in the present study we have used $N = 30$ for computation of Lagrangian particle trajectories.

The particle trajectories have been obtained as following. For the four neighboring grid points of the particle position at $t = t$, the velocity components u_ξ, u_η are obtained by (13). Then (u_ξ, u_η) of the (ξ, η) coordinate system are transformed to (u_x, u_r) of the (x, r) coordinate system. The new position of the particle is obtained by integrating (11) with the explicit Euler method. If the particle position is not exactly at a grid point, the velocity components are obtained by the bilinear interpolation of the values at the four neighboring points. The time step used in integration is $\Delta t = 10^{-4}$.

4. Results and discussion

4.1. Unsteady flow fields and mass transfer

We have studied the dynamical flow patterns and the unsteady mass transfer for pulsatile flows in an axi-

symmetric wavy channel in the range of $50 \leqslant Re \leqslant 250$ and $0.1 \leqslant St \leqslant 10$. We chose the range of the Reynolds number for which the fluid flow is expected to be laminar. For the range of the Strouhal number, some previous workers [4, 6, 9] considered the cases of low Strouhal number in the range $O(10^{-4})$–$O(10^{-1})$, and some others considered moderately high Strouhal numbers in the range $O(10^{-2})$–$O(1)$ [5, 10]. Especially Nishimura and Kojima [5] performed their experiments up to the Strouhal number $St = 1.5$. (In their definition, the largest value was six. Although their geometry is 2-D and ours is axisymmetric, if the two definitions are compared based on the mean inlet velocity we can see that there is a factor of 4 between their definition and our definition.) As mentioned in the Introduction, however, their Strouhal number range was not high enough to find the optimal Strouhal number for the mass transfer enhancement. Thus, in the present study, we chose the range mentioned above in the hope that we find an optimal Strouhal number.

Streamlines at the specified times of one period are shown in Fig. 6 for the case of $Re = 250$, $St = 2$, $\Omega_w = 1$ with the inlet velocity profile given in Fig. 2 ($\varepsilon = 0.2$). The flow field has a 2π-periodicity due to the 2π-periodic inlet flow condition. Thus the flow field is quite regular in the Eulerian point of view. However, in the Lagrangian point of view, the particle trajectories show very complicated behaviors as will be shown later.

At $t = 0$ (here t is measured after the fully time-periodic flow field is obtained), there is a rotating flow in the counterclockwise because of the decelerating flow during $\pi \leqslant t \leqslant 2\pi$ of the previous period. As the time increases from $t = 0$ to π, the flow field is accelerated and the x-directional pressure gradient ($\partial p/\partial x$) becomes negative more and more, and the counterclockwise vortex is diminished and swept downstream as shown for $t = \pi/4$ and $\pi/2$. However, as the flow rate increases further, the pressure at the diverging section increases and the pressure is built-up near the point of maximum cross section. The reversing pressure gradient makes a new recirculating flow as seen in Figs 6(d) and (e). When $\pi < t < 2\pi$, the reversing pressure gradient, i.e. $(\partial p/\partial x) > 0$ is built-up and the recirculating flow becomes stronger as shown for the cases of $t = 5\pi/4$ and $3\pi/2$. As the flow rate decreases further, the vortex is ejected from the wall and it is bulged out to occupy the entire channel. This behavior is possible because the continuity of stress of viscous fluid ensures that the moving fluid entrains stationary fluid before the whole fluid would come to rest. The growth, diminishing, and ejection of the vortex result in the complicated particle trajectories and the mass transfer enhancement as will be shown later.

Figure 7 shows the instantaneous concentration profiles during one period under the same conditions for the flow field in Fig. 6 with the Schmidt number $Sc = 1$. The concentration profile is 2π-periodic due to the periodicity

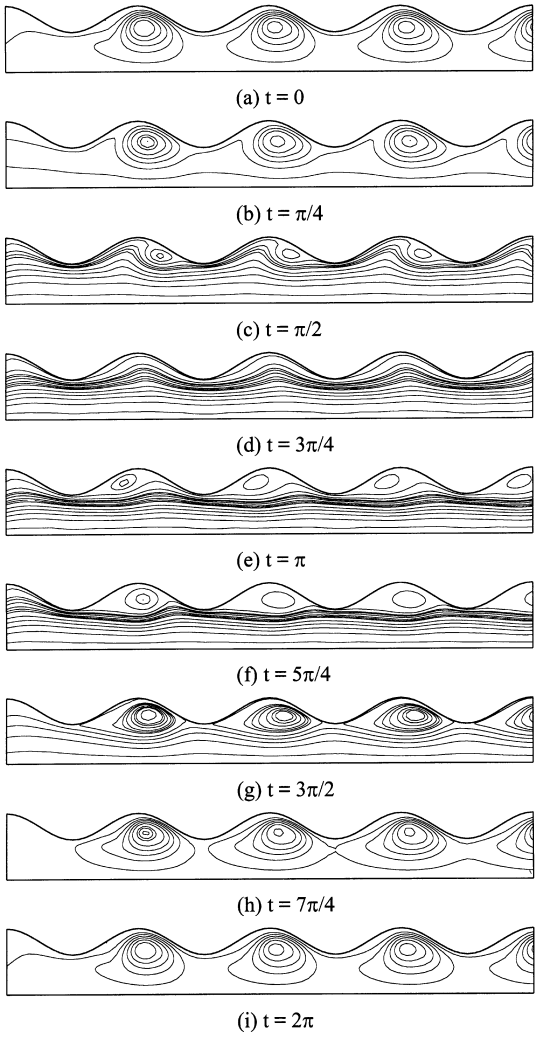

Fig. 6. Instantaneous streamlines during one period when $Re = 250$, $St = 2$, $\Omega_w = 1.0$, and $\varepsilon = 0.2$.

of the flow field. In this case, the mass transfer Peclet number is $Pe = Re \cdot Sc = 250$ and the convection effect is dominant. Thus as shown in the figure, the concentration profile is highly coiled when there are circulating vortices. This behavior is expected to enhance the mass transfer rate. In the next subsection, the mass transfer enhancement is discussed in a quantitative sense.

4.2. Mass transfer enhancement by unsteady mixing

The mass transfer enhancement factor E was introduced in Section 2 in order to represent how much the transport is enhanced by the pulsatile flow in a wavy channel. In Fig. 8, the mass transfer enhancement factor is shown as a function of the Strouhal number for several values of the Reynolds number when $Sc = 1$, $\Omega_w = 1$

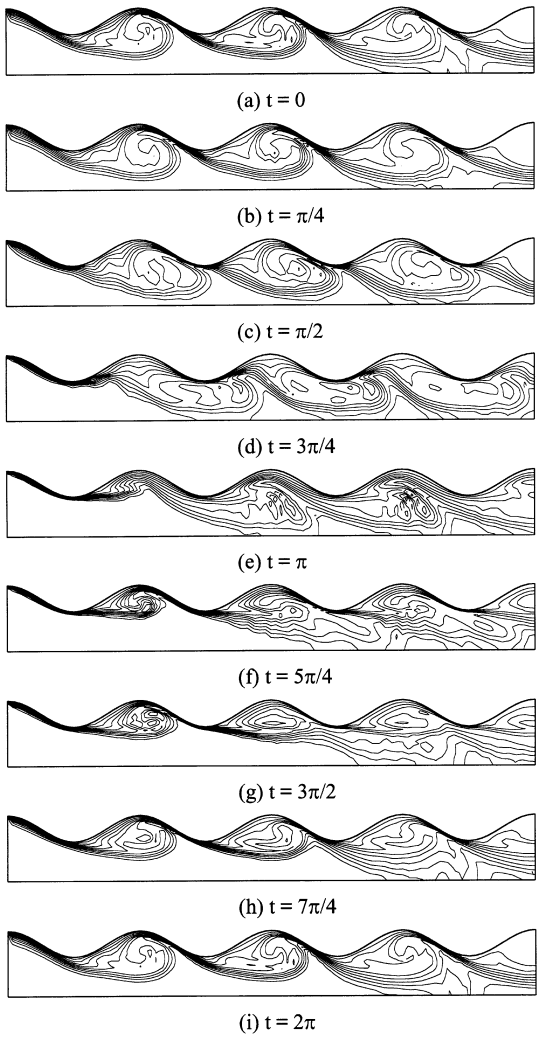

Fig. 7. Instantaneous concentration profiles when $Re = 250$, $St = 2$, $Sc = 1$, $\Omega_w = 1.0$, and $\varepsilon = 0.2$.

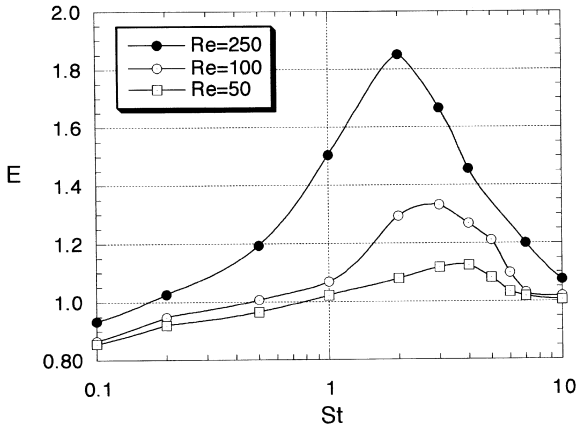

Fig. 8. The effect of the Strouhal number on the mass transfer enhancement factor for different Reynolds numbers when $\Omega_w = 1.0$, $Sc = 1$, and $\varepsilon = 0.2$.

with the pulsation amplitude $\varepsilon = 0.2$. Since the Strouhal number is proportional to the pulsation frequency, we may regard the results as the pulsation frequency effects on the mass transfer enhancement. From the figure, we can observe two facts. One is that the mass transfer enhancement increases as the Reynolds number increases. This fact is self-explanatory because the dynamical nature of the fluid flow, which results in the mass transfer enhancement, becomes stronger as the Reynolds number increases. The same trend has also been observed by the previous workers (for example, Nishimura et al. [4], Nishimura and Kojima [5]).

The second fact is that there exists an optimal Strouhal number for each Reynolds number, and that the optimal Strouhal number deceases as the Reynolds number increases. The trend may be explained by the fact that less energy is required to excite the velocity field as the energy loss due to viscous dissipation decreases. Even though not directly applicable to the present study, the results of Ghaddar et al. [2] is worth mentioning. In their study on the flow in grooved channels, they computed the least-stable grooved-channel mode and found that the oscillation frequency decreases as the Reynolds number increases. If the least-stable mode is excited most easily, we may expect that the fluid mixing is enhanced at or near the frequency of the mode.

Te second fact mentioned above has not been reported for the 2-D or axisymmetric wavy channel problem and there are several things to be noted. One is that the optimal Strouhal number is $O(1)$ for the Reynolds number range considered in this study. As mentioned earlier, Nishimura and Kojima [5] observed from their experiments that the enhancement factor increases as the Strouhal number increases. However, the range of their Strouhal number was not high enough to detect the optimal value. Since the experiments of Nishimura and Kojima [5] are for the 2-D geometry with $\Omega_w = 0.7$, the direct comparison of their results (their Fig. 10) with the results from the present study is not possible. However, the enhancement factor at their $Re = 292$ and $St = 6$ (in our definition $Re = 292$, $St = 1.5$) is about 1.7 when they used the pulsation amplitude parameter $P = 1$ (at this parameter, the system is about to have a backward flow). This fact shows that the results obtained in the present study is reasonable. In Fig. 8, there is one more fact to be mentioned. When the Strouhal number is very small (e.g. 0.1), the enhancement factor becomes less than one. This is possible because the reference problem is for the mass transfer in steady flow, in which there is no flow oscillation [see the definition in equation (9)]. On the other hand, in the case of pulsatile flow with a very small Strouhal number, the problem can be regarded as a quasi-

steady state problem. However, during one period, it experiences many different values of the inlet velocity. Thus the average does not have to be the same as that for the reference problem.

Since the results in Fig. 8 were obtained for the pulsatile flow with small backward flow (the pulsation amplitude in equation (6) is $\varepsilon = 0.2$ and see also Fig. 2), we have the question of whether the same behavior is obtained for the pulsatile flow with smaller amplitude that does not produce backward flow. To answer the question, we performed the same analysis for the case of $\varepsilon = 0.1$. In this case, there is no backward flow and the range of the inlet velocity is $0.3 \leqslant u_x \leqslant 1.7$ [see equation (6)]. From the results, we found that the optimal values of the Strouhal number are not changed even though the enhancement factor for each Reynolds number is decreased (the results are not shown).

The effect of the geometric wave number on the optimal Strouhal number has also been studied. In Fig, 9, the enhancement factor is plotted as a function of the Strouhal number for various geometric wave numbers. For the range of $0.5 \leqslant \Omega_w \leqslant 1.5$, the optimal Strouhal number is almost proportion to the geometric wave number. Since the wall wavelength is inversely proportional to the geometric wave number, the optimal Strouhal number is almost inversely proportional to the wall wavelength. This fact suggests that the mass transfer is most enhanced by the vigorous mixing when the pulsation time scale is more or less proportional to the time scale required for convection of excited fluid elements to the next wavy region of the channel.

Thus far, we have seen that there exists an optimal Strouhal number when other parameters are fixed. Now it is appropriate to explain the maximum transport enhancement at a certain pulsation frequency through

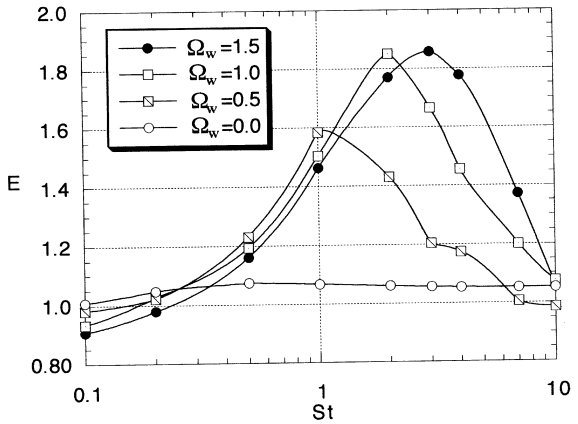

Fig. 9. The effect of the Strouhal number on the mass transfer enhancement factor for different geometric wave numbers. *Re* and *Sc* are fixed as $Re = 250$ and $Sc = 1$ ($\Omega_w = 0.0$ corresponds to the cylindrical channel).

the physical processes. The previous works on the resonant heat transfer enhancement in a periodically grooved channel [1–3] indicate that the hydrodynamic resonance takes place when the imposed frequency is the same as the natural frequency for the self-sustained oscillation due to Tollmien–Schlichting waves. They also showed that there exists a least-stable frequency that could be excited most easily even at the Reynolds numbers below the critical value for the self-sustained oscillation. Although the geometry considered in this study is not exactly the same as the grooved channel, the present problem shares several common aspects with the groove problem and the transport enhancement can also be explained by the concepts of hydrodynamic instabilities. Under steady condition, there exist separating flows in an axisymmetric wavy channel as in a grooved channel. Thus, if this basic flow field is perturbed at sub-critical Reynolds numbers, the flow would exhibit damped oscillation at the frequency of the least-stable mode. Now, in the case of pulsatile flow with a certain mean flow rate, the strongest response is expected when the pulsation frequency is near the frequency of the least-stable mode of the perturbed flow about the steady flow field. Because of this hydrodynamic resonance, the flow field becomes most complicated and results in vigorous fluid mixing across the streamlines that would be obtained if the flow field is steady. In this way, maximum transport enhancement is obtained at a certain pulsation frequency.

The dependency of the optimal Strouhal number on the geometric wave number can also be explained by the hydrodynamic resonance. Ghaddar et al. [2] studied the geometric dependence of the selection of the least-stable for the grooved channel flows. Among the parameter sets they studied, the most relevant ones to the present study are for the cases of $L/l = 2$, where L is the length of one-periodic unit and l is the length of the groove part (see their Table 1). For these cases, they showed that the perturbed flow has one wave in a periodic unit and that the frequency of the least-stable mode is almost inversely proportional to L. Although the geometry in this problem is not exactly the same as those, we can expect a similar result for the present problem. Thus, we may anticipate that the least-stable mode is also inversely proportional to the geometric wavelength of the channel (or nearly proportional to the geometric wave number). Therefore the Strouhal number of the maximum enhancement is expected to be almost proportional to the geometric wave number as shown in Fig. 9.

4.3. Lagrangian characterization of flow fields

In the above, we have explained the maximum transport enhancement at a certain pulsation frequency based on the concepts of the hydrodynamic resonance. However, since the key to high mass transfer rate is the convective transport and fluid mixing induced by the

pulsatile flow, we want to characterize the flow fields by using the concepts of the non-linear dynamics and the Lagrangian dynamics in order to understand the mass transfer enhancement better. First we take a look at the trajectories of (massless noninteracting point) particles to see the qualitative nature of fluid mixing. Then we analyze the flow field by using the Lagrangian Lyapunov exponent for characterization in the quantitative sense.

4.3.1. Chaotic particle trajectories

Trajectories of 6 test particles are shown in Fig. 10 for different Strouhal numbers when $Re = 250$, $\Omega_w = 1$ and $\varepsilon = 0.2$. From the figure, we can see that the particle motions are relatively simple in the case of very high or very low Strouhal number. On the other hand, in the cases of $St = 2$, 3, and 1, the particle motions are quite complicated. The complicated motion is due to the vortex formation, growing and ejection as discussed in the previous subsection. Especially, it is worthwhile to note that even the particles starting from the center region of the channel are entrained to the region near the wall after a certain time. It would be of particular interest if we note also that there is a strong correlation between the complexity of particle trajectories near the wall and the mass transfer enhancement (see the case of $Re = 250$ in Fig. 8).

To investigate diffusive transport of the particles, we float a blob of 1000 particles on the flow, and trace their displacements along the traveling time. Figure 11 is for the case of $Re = 250$, $St = 2$, and $\varepsilon = 0.2$. The degree of dispersion is measured by the variance σ^2 defined by $\sigma^2 = \Sigma_i[(x_i - x_m)^2 + (r_i - r_m)^2]$ where $x_m = \Sigma_i x_i/n$, $r_m = \Sigma_i r_i/n$ and n is the number of particles. From the figure, we can see that the dispersion process is affected by the circulating flows generated in the wavy region. When the particles reach a valley of channel at time $t = 8$–10, a portion of particles is separated from the main body of the blob. It is due to the saddle mode occurring in a valley of the channel.

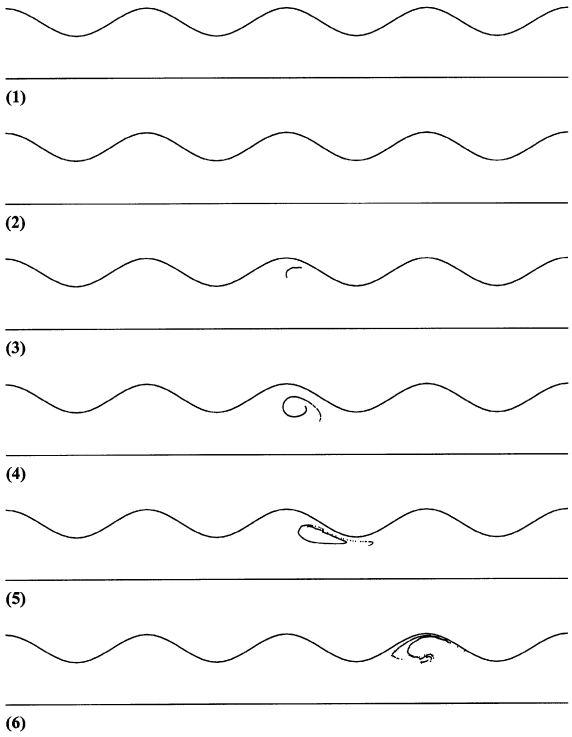

Fig. 11. Displacement of a blob of 1000 particles in the case of $St = 2$ and $Re = 250$: (1) the blob starts at $t = 0$, (2) $t = 2$ and the variance $\sigma^2 = 1.30$, (3) $t = 4$ and $\sigma^2 = 4.27$, (4) $t = 6$ and $\sigma^2 = 19.45$, (5) $t = 8$ and $\sigma^2 = 60.72$, (6) $t = 10$ and $\sigma^2 = 90.99$.

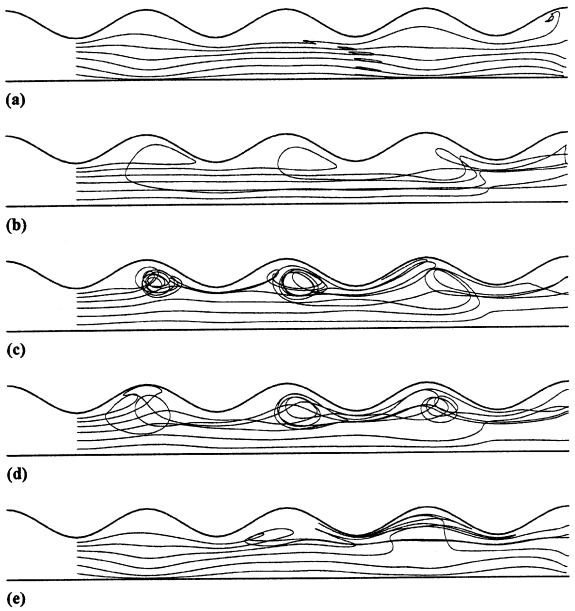

Fig. 10. Particle trajectories obtained for the cases of different Strouhal numbers when $Re = 250$, $\Omega_w = 1.0$, and $\varepsilon = 0.2$: (a) $St = 0.1$, (b) $St = 1$, (c) $St = 2$, (d) $St = 3$ and (e) $St = 10$.

4.3.2. Lagrangian Lyapunov exponent

We have computed the Lagrangian Lyapunov exponent along the grid lines near the wall to quantify the mixing efficiency following Amon et al. [14]. According to their idea, the Lagrangian Lyapunov exponent λ_L estimates the rate at which the distance between two initially infinitesimally close test particles increases or decreases with time. It is defined as

$$\lambda_L = \frac{1}{N}\sum_{k=1}^{N}\lambda_k, \quad \lambda_k = \frac{1}{t^k - t_0^k}\ln\left(\frac{d^k}{d_0^k}\right) \tag{15}$$

where $d_0^k = \|\mathbf{x}_1(t_0^k) - \mathbf{x}_2(t_0^k)\|$ and $d^k = \|\mathbf{x}_1(t^k) - \mathbf{x}_2(t^k)\|$

are the initial and final distances between two test particles, respectively, and N is the number of times that this operation is repeated for a continuous time evolution of the Eulerian velocity field. In this study, we have used $d_0^k = 5\times10^{-5}$, $t^k - t_0^k = 0.25$, and $N = 50$ (so the time required for repeating 50 times covers approximately two periods of pulsation).

The spatial distribution of the Lyapunov exponent λ_L for the case of $Re = 250$, $St = 2$, $\Omega_w = 1$, and $\varepsilon = 0.2$ is shown in Fig. 12. A set of particle pairs were initially positioned along the grid line $j = 18$ (the grid line $j = 21$ corresponds to the wall). In the figure the points $x = 3$ and $x = 5$ correspond to the smallest diameter section and $x = 4$ the largest diameter section (see Fig. 3). We can see that the stretching of fluid element is strong in the larger diameter region because of the vortex formation, growth, and ejection, etc. Since the stretched fluid element is folded by being bent as can be seen in Fig. 11, the high value of λ_L indicates active mixing.

Since λ_L represents the local behavior of fluid element, we define the average finite-time Lagrangian exponent $\bar{\lambda}_L$ in order to find some relationship between $\bar{\lambda}_L$ and the mass transfer enhancement factor E. To obtain $\bar{\lambda}_L$, we first locate a set of particle pairs along grid line near the wavy wall, for example the grid points (31, 19), (32, 19), ..., (49, 19). Then we compute λ_L for all those particle pairs and average them as $\bar{\lambda}_L = (\Sigma_{k=1}^{n} \lambda_L)/n$.

If mixing efficiency is determined by the stretching rate, it should be directly related to $\bar{\lambda}_L$. In Fig. 13, the average Lagrangian Lyapunov exponent is shown as a function of the Strouhal number for the case of $Re = 250$, $\Omega_w = 1$, and $\varepsilon = 0.2$ (the same flow conditions as those for the closed circles in Fig. 8). As we can see in the figure, $\bar{\lambda}_L$ has maximum at $St = 3$ and becomes smaller as the Strouhal number increases to $O(10^1)$ or decreases to $O(10^{-1})$. Now by comparing Fig. 13 and Fig. 8, we can see that the behaviors of the mass transfer enhancement factor E and the average Lagrangian Lyapunov exponent $\bar{\lambda}_L$ are very similar even though the optimal Strouhal numbers are not exactly the same. This fact suggests that there is a strong correlation between the mass transfer enhancement factor and the average Lagrangian Lyapunov exponent.

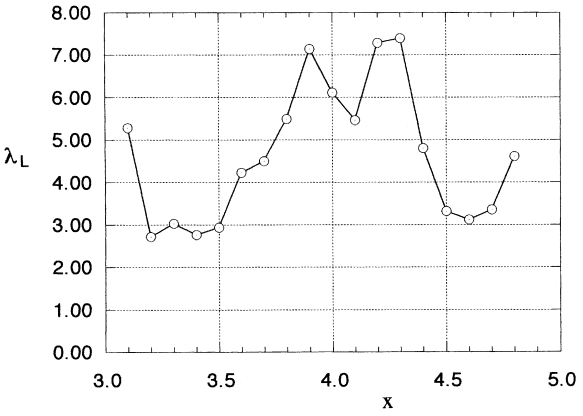

Fig. 12. Spatial distribution of the finite-time Lagrangian Lyapunov exponents λ_L along the grid line $j = 18$ in the case of $Re = 250$, $St = 2$, $\Omega_w = 1.0$, and $\varepsilon = 0.2$.

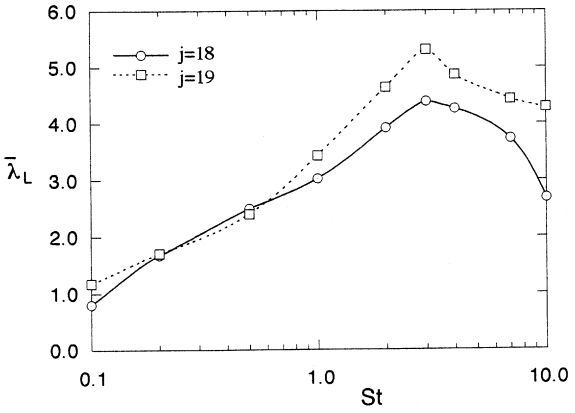

Fig. 13. The effect of the Strouhal number on the average Lagrangian Lyapunov exponent $\bar{\lambda}_L$ ($j = 18$ represents the 18th grid line in the radial direction and $j = 19$ the 19th grid line) when $Re = 250$, $\Omega_w = 1.0$, and $\varepsilon = 0.2$.

5. Conclusions

We have investigated numerically the mass transfer enhancement by a pulsatile flow in an axisymmetric wavy channel for the range of $50 \leqslant Re \leqslant 250$ and $0.1 \leqslant St \leqslant 10$. The optimal Strouhal number for mass transfer enhancement has been determined as a function of the Reynolds number and the wavelength of the channel. For better understanding of the enhancement mechanism, the Lagrangian flow analysis has also been performed. For an efficient particle trajectory computation, the Eulerian velocity field is represented by the Fourier series. From the results of the present study we have reached the following conclusions:

(1) The optimal Strouhal number is $O(1)$ and is a weak decreasing function of the Reynolds number.
(2) Another important factor to the optimal Strouhal number is found to be the wavelength of the channel. The optimal value of the Strouhal number is almost inversely proportional to the wavelength of the channel.
(3) Particle trajectories show chaotic behaviors when the Strouhal number is close to the optimal value. It is also observed that there is a very strong correlation between the mass transfer enhancement factor and the average Lagrangian Lyapunov exponent.

Acknowledgments

This work has been supported by a grant from the Korea Science and Engineering Foundation through the Advanced Fluids Engineering Research Center at the Pohang University of Science and Technology. The authors would like to acknowledge their financial support.

References

[1] A.T. Patera, B.B. Mikic, Exploiting hydrodynamic instabilities. Resonant heat transfer enhancement, Int. J. Heat Mass Transfer 29 (1986) 1127–1138.
[2] N.K. Ghaddar, K.Z. Korczak, B.B. Mikic, A.T. Patera, Numerical investigation of incompressible flow in grooved channels. Part 1. Stability and self-sustained oscillations, J. Fluid Mech. 163 (1986) 99–127.
[3] N.K. Ghaddar, M. Magen, B.B. Mikic, A.T. Patera, Numerical investigation of incompressible flow in grooved channels. Part 2. Resonance and oscillatory heat transfer enhancement, J. Fluid Mech. 168 (1986) 541–567.
[4] T. Nishimura, A. Tarumoto, Y. Kawamura, Flow and mass transfer characteristics in wavy channels for oscillatory flow, Int. J. Heat Mass Transfer 30 (1987) 1007–1015.
[5] T. Nishimura, N. Kojima, Mass transfer enhancement in a symmetric sinusoidal wavy-walled channel for pulsatile flow, Int. J. Heat Mass Transfer 38 (1995) 1719–1731.
[6] I.J. Sobey, On flow through furrowed channels. Part 1. Calculated flow patterns, J. Fluid Mech. 96 (1980) 1–26.
[7] K.D. Stephanoff, I.J. Sobey, B.J. Bellhouse, On flow through furrowed channels. Part 2. Observed flow patterns, J. Fluid Mech. 96 (1980) 27–32.
[8] I.J. Sobey, The occurrence of separation in oscillatory flow, J. Fluid Mech. 134 (1983) 247–257.
[9] M.E. Ralph, Oscillatory flows in wavy-walled tubes, J. Fluid Mech. 168 (1986) 515–540.
[10] Y. Jeong, I.S. Kang, Pulsatile flows in stenosed blood vessels, Korean J. of Chem. Eng. 12 (1995) 540–550.
[11] A. Kaneko, H. Honji, Double structures of steady streaming in the oscillatory viscous flow over a wavy wall, J. Fluid Mech. 93 (1979) 727–736.
[12] P. Hall, Unsteady viscous flow in a pipe of slowly varying cross-section, J. Fluid Mech. 64 (1974) 209–226.
[13] A.M. Guzman, C.H. Amon, Dynamical flow characterization of transitional and chaotic regimes in converging–diverging channels, J. Fluid Mech. 321 (1996) 25–57.
[14] C.H. Amon, A.M. Guzman, B. Morel, Lagrangian chaos, Eulerian chaos, and mixing enhancement in converging–diverging channel flows, Phys. Fluids 8 (1996) 1192–1206.
[15] J.M. Ottino, Mixing, chaotic advection, and turbulence, Annu. Rev. Fluid Mech. 22 (1990) 207–253.
[16] L.G. Leal, Laminar Flow and Convective Transport Process, Butterworth-Heinemann, Boston, 1992, pp. 105–113.
[17] H.J. Oh, I.S. Kang, A non-iterative scheme for orthogonal grid generation with control function and specified boundary correspondence on three sides, J. Comput. Phys. 112 (1994) 138–148.